Coupling of Carbonate Associated Sulfate and Carbon Isotope Trends in Middle Ordovician Strata from Meiklejohn Peak, Nevada: Implications for atmospheric O_2

Undergraduate Thesis

Presented in Partial Fulfillment of the Requirements for graduation "with Research Distinction in Earth Sciences" in the undergraduate colleges at The Ohio State University

Natasha Lewis

The Ohio State University

Spring, 2014

Project advisor: Dr. Matthew Saltzman, School of Earth Sciences

Table of Contents Page

Figures

Abstract

Dramatic increases in biodiversity of marine animal life occurred throughout the Middle Ordovician period. To understand the origin of this biodiversity pulse, a stratigraphic unit of the Middle Ordovician Antelope Valley Limestone (AVL) at Meiklejohn Peak, Nevada was examined for $\delta^{34}S_{CAS}$ and $\delta^{13}C_{carb}$, which are proxies for the burial rate of pyrite sulfur and organic carbon, respectively. Results indicate positive trends in both $\delta^{34}S_{CAS}$ and $\delta^{13}C_{carb}$ through the upper middle member of the AVL. I interpret these trends to represent a rise in sea level leading to increased pyrite burial rates, decreased weathering of terrestrial pyrite deposits, and an increase in bacterial sulfate reduction (BSR) in anoxic waters. A previous $\delta^{13}C_{carb}$ study at Meiklejohn Peak, Nevada hypothesized that the observed positive shift in $\delta^{13}C_{carb}$ represents an increase in burial of organic carbon that led to a period of increased atmospheric oxygen concentration. Increased oxygen levels may have acted as a causal mechanism for coeval biologic radiations. The $\delta^{34}S_{CAS}$ data presented herein support the hypothesis of an increase in Middle Ordovician atmospheric oxygen.

Introduction

Throughout Earth history, a proxy record of oceanic and atmospheric oxygen levels is preserved in the stable isotopic compositions of carbon and sulfur in carbonate rocks (Gill et al., 2007). Carbonate depositional sequences containing these chemical signatures also record coeval climatic, environmental, and biologic changes that may reveal a causal relationship with oxygen levels (Mackenzie and Pigott, 1981; Canfield and Raiswell, 1999; Gill et al., 2007). Use of these carbon and sulfur isotope proxies has allowed for the examination of past oxygenation events in paleo-Earth systems such as shifts observed in correlation with Snowball Earth, the biologic radiation in the Ediacaran, the Cambrian Explosion, and other fluctuations throughout the Paleozoic (Canfield and Raiswell, 1999; Kah et al., 2004; Gill et al. 2007; McFadden et al., 2008).

Application of sulfur isotopes in carbonate rock ($\delta^{34}S_{CAS}$) as a chemical proxy is limited by technological constraints on isotope detection, preservation of primary seawater values, and correlation of stratigraphic units regionally or globally (Wotte et al., 2012). Abundant unconformities and other controls on meteoric diagenesis must be carefully evaluated before the observed isotopic trends can be interpreted as primary (Gill et al., 2008; Edwards and Saltzman, 2014). This study utilizes an extraction methodology based upon Gill et al. (2011) and Wotte et al. (2012) that is designed to minimize the effects of secondary alteration of seawater values in carbonate associated sulfate (CAS).

Oceanic sulfur exists in two primary reservoirs-sulfate and sulfide (e.g. as pyrite, FeS_2)-representing oxidized and reduced forms, respectively (Mackenzie and Pigott, 1981; Gill et al., 2007; Lyons and Gill, 2010). The exchange between these reservoirs can be investigated using

stable isotopes (Mackenzie and Pigott, 1981). Here I examine the interaction of these sulfur reservoirs utilizing carbonate associated sulfate (CAS) signatures from Middle Ordovician strata that formed in an outer carbonate ramp setting and now outcrop at Meiklejohn Peak, Nevada (Ross, 1977; Edwards and Saltzman, 2014). Preliminary results suggest positive correlation between $\delta^{34}S_{CAS}$ and previously procured $\delta^{13}C_{carb}$ isotope data. Cotetaneous $\delta^{13}C_{carb}$ data tracks a $\delta^{34}S_{CAS}$ shift of 1.61‰ and 1.94‰, respectively, through the upper middle member of the Antelope Valley Limestone (AVL). I attribute the causal mechanism behind these chemostratigraphic changes to be a result of a rise in sea level and resultant increase in burial rates of both organic carbon and pyrite, which subsequently induced the rise of atmospheric oxygen.

Background: The geochemical sulfur cycle

Sulfate reducing bacteria found in both modern and ancient oceans fractionate sulfur isotopes with a preference for the naturally stable lighter isotope (^{32}S), and expel reduced sulfide as part of bacterial sulfate reduction (BSR) (Mackenzie and Pigott, 1981; Canfield and Raiswell, 1999; Gill et al., 2007). In the presence of certain metal elements, this reduced compound (HS^-) forms metal (M^{2+}) sulfides (e.g., pyrite FeS_2), which may then become buried within the sedimentary record (Mackenzie and Pigott, 1981; Canfield and Raiswell, 1999; Gill et al., 2007). The residual sulfate in the oceans is left isotopically heavier and is incorporated into carbonate associated and evaporative sulfates, providing a direct record of past ocean water composition (Mackenzie and Pigott, 1981; Canfield and Raiswell, 1999; Gill et al., 2007). Sulfate reservoir inputs originate from continental weathering and subsequent oxidation of terrestrial sulfide components (e.g., pyrite deposits) and from volcanic sources, both marine and continental

(Mackenzie and Pigott, 1981; Gill et al., 2007). The extent to which reduced sulfur oxidizes is proportional to the amount of oxygen available in the paleoatmosphere, which also relates to the evolution of aerobic organisms (Kah et al., 2004; Gill et al., 2007; Lyons et al., 2010; Webby et al., 2010). While other factors influence the oxidation of terrestrial sulfides, including the local pH, supply of ferric iron (in alkaline settings), temperature, bacteria activity, and the crystal structure of pyritic material, the role of atmospheric oxygen is most readily interpreted when utilizing paleo-proxies (Nicholson et al., 1988; Gill et al., 2007). The signatures associated with $\delta^{34}S_{CAS}$, therefore, can reveal details about the evolution of atmospheric oxygen conditions throughout Earth history (Canfield and Raiswell, 1999; Kah et al., 2004; Gill et al., 2007; Lyons et al., 2010).

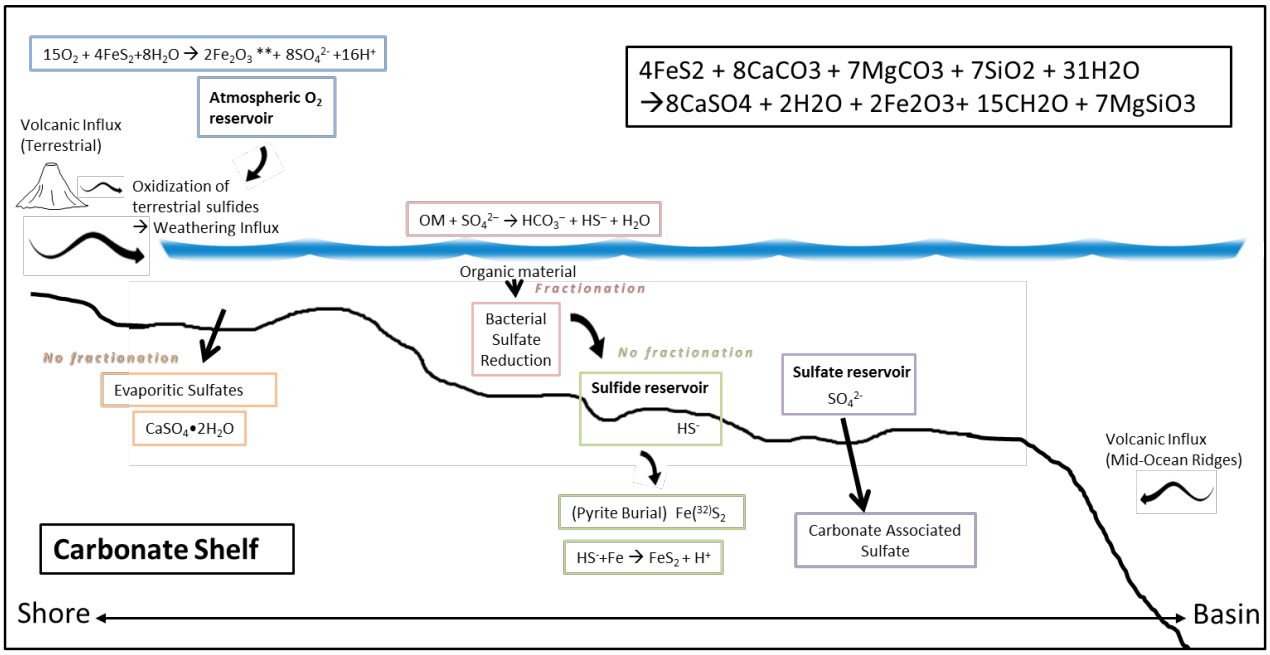

Figure 1: Bacterial sulfate reduction (BSR) is found at the modern-day oceanic sediment-water interface (but may have also occurred in the water column in euxinic/anoxic bottom waters in the Paleozoic oceans). Sulfate reducing bacteria fractionate sulfur with preference to the lighter stable isotope (^{32}S), as they turn organic matter (OM) into energy through a process that reduces sulfate into sulfide (e.g., HS^-). As a result of BSR, the sulfide reservoir is enriched in the light isotope of sulfur. These sulfides then react with metals, prominently iron, to form metal M^{2+} sulfides (e.g., FeS_2). Oxidation of terrestrial sulfides, such as those found in exposed pyrite deposits, through weathering is a source of isotopically light sulfur into the oceans. Both terrestrial and mid-ocean ridge (MOR) volcanism input light (^{32}S) isotopes into the atmospheric and oceanic systems. There is no fractionation of the sulfate reservoir associated with the formation of carbonate associated sulfate (CAS) or evaporative salts such as gypsum and anhydrite. The sulfur isotopic composition of ocean water is influenced by pyrite burial and weathering, and therefore may indicate shifts in atmospheric oxygen over time. (Gill et al., 2007)

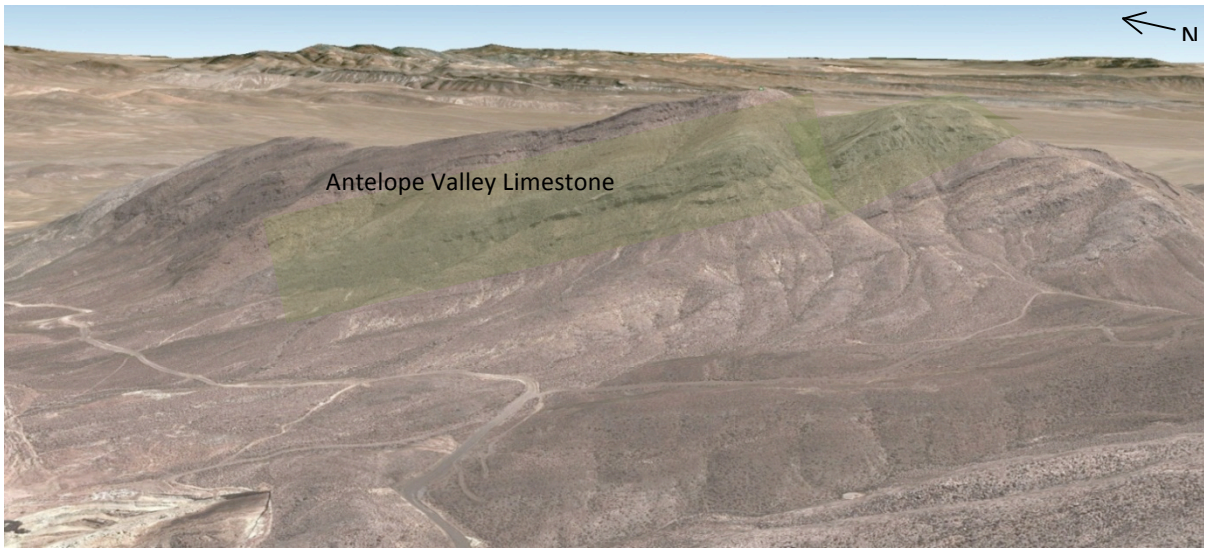

Figure 2: Google Earth image of the field section (see Diamond, 2013 for details of the path of sample collection). The general part of the section containing the Antelope Valley Limestone (AVL) is highlighted in green and lies beneath the Eureka Quartzite.

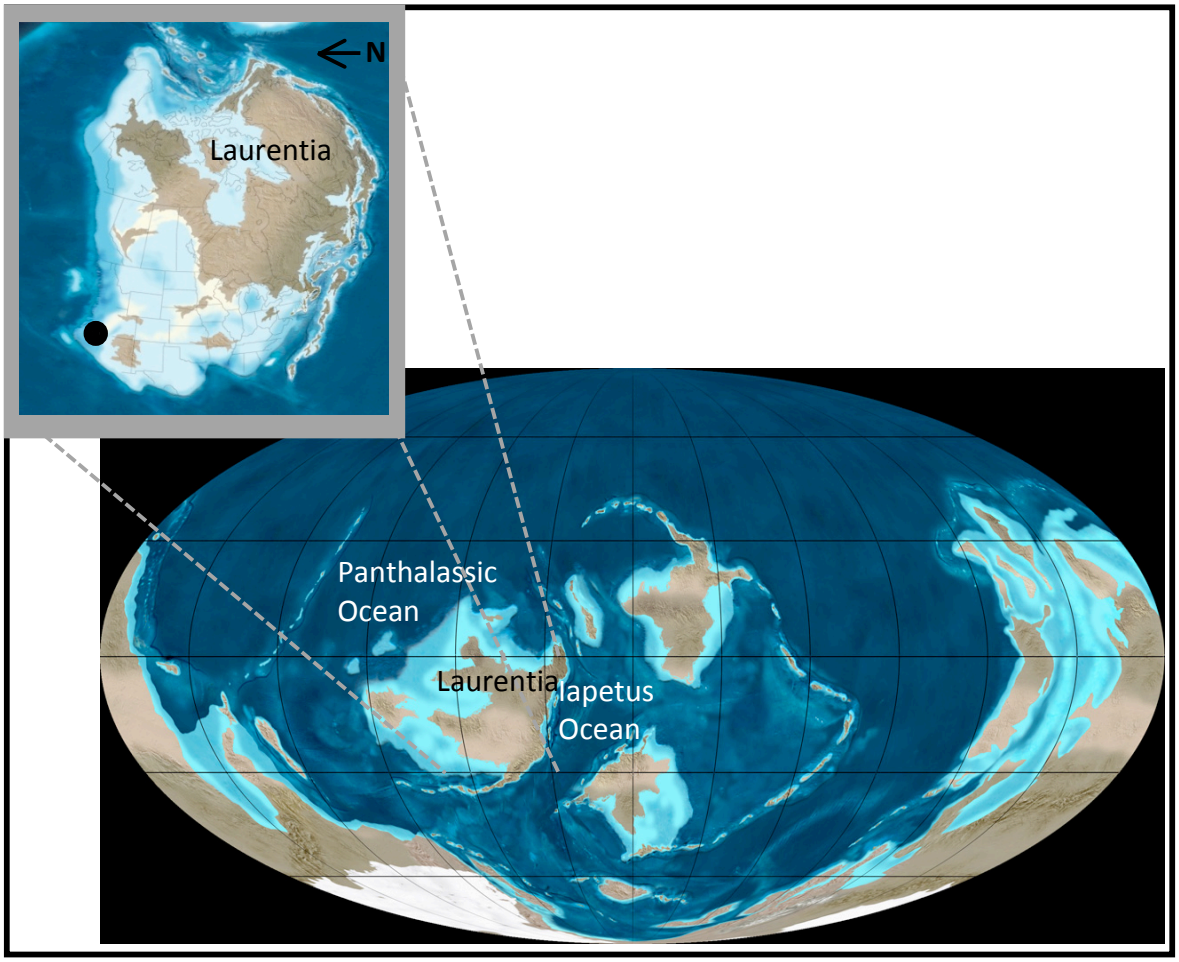

Figure 3: Paleogeographic map of the Middle Ordovician presented by Dr. Ron Blakey (http://cpgeosystems.com/namO470.jpg; http://cpgeosystems.com/470moll.jpg). Inset shows field area Meiklejohn Peak (MP) marked on an outer shelf of the Laurentian continent within an overlay of modern N. America.

Geologic Setting

Conodont study of the Antelope Valley Limestone (AVL) at Meiklejohn Peak, Nevada indicates a Darriwilian stage age during the Middle Ordovician (Harris, 1979; Webby et al., 2004; Young et al., 2009). In addition, the Antelope Valley Limestone records the Middle Darriwilian Isotopic Carbon Excursion (MDICE) (Diamond, 2013), which is consistent with the presence of the *Eoplacognathus suecicus* conodont zone (Harris, 1979). Underlain by the Nine Mile Shale, the Antelope Valley Limestone (AVL) is overlain by the Eureka Quartzite (Ross, 1977). This overall stratigraphic sequence records a progressive shallowing upwards from outer to inner carbonate ramp environments, culminating in a large scale influx of quartz sand.

The AVL formed on a shallow carbonate platform conducive to diverse marine animal life and isolated from clastic intrusion (Ross, 1977). The lower and middle members of the AVL contain various fragmented trilobite and brachiopod remains. Ross (1977) interprets the lower member, occurring just below the study section, as subtidal based on fossil-rich muddy packstone lithofacies that continues part way through the middle member. Around 371.5 cumulative meters (within the middle member), the facies shift to mud supported wackestone, with diminishing fossil occurrences. The transition between the middle and upper Harris members marks a rapid change from muddy wackestone to crystalline mudstones. The ensuing Eureka quartzite records a deluge of siliciclastic materials transported from the mid-continent (Ross, 1977). As marked in Figure 3, the study section lies upon a passive margin along the outer edge of the Laurentian continental shelf (Bond et al., 1984). Following the breakup of Rodinia, the continental remnant of Laurentia began to drift from equatorial regions to 30° south latitude, creating a dramatic change in climate and causing the formation of epeiric seaways home to vast expanses of carbonate platforms (Ross, 1977).

Figure 4: Images of rock samples powdered for $\delta^{34}S_{CAS}$. From left to right samples occurring at 322, 352, 379, 389.5, 404.5, ad 410.5 cumulative meters (see Figure 7). Oldest samples (lower meterage) are composed of muddy grain supported packstones (often peloidal), with up to 15% sparry calcite and calcite veins, and containing fossil brachiopod and trilobite fragments. A shift occurs at 371.5 cumulative meters (between samples b and c), marked by a conversion to mud supported wackestone. Red and tan clays are common throughout the section.

Methods

A 270-meter-thick interval of the Harris Section of the Antelope Valley Limestone exposed at Meiklejohn Peak, Nevada (Harris, 1979) was sampled at a 1.5 meter spacing using a Jacob's staff (Diamond, 2013). From this sampled interval, 100 samples were analyzed for $\delta^{13}C$ measured from unaltered micrite according to methods described by Saltzman et al. (1998) (see also Saltzman, 2003; Saltzman and Young, 2005). A total of 21 samples were selected for CAS analysis based upon three qualifications: adequate size of the sample capable of producing at least 80 g of unweathered carbonate, even spacing of roughly 10-15 meters within the section, and previously measured $\delta^{13}C$ data associated with the sample. Each sample was then cut, pulverized, and processed following methodology drawn from Gill et al. (2011) and Wotte et al. (2012).

Samples were rinsed using about 400 mL of 10% NaCl solution in order to dissolve and remove any sulfate minerals (e.g., gypsum and anhydrite). Samples were processed in two groups: Group 1 consisted of 10 samples from the bottom of the section (approximately 320 to 410 cumulative meters), and went through the NaCl rinsing process only once; Group 2 consisted of the upper 11 samples (approximately 410 to 560 cumulative meters) and went through the NaCl rinsing process twice. Each sample was then rinsed with 500 mL of 18 MΩ (Milli-Q) water to remove any dissolved sulfate. Samples were treated with 300 mL of 6% NaClO (bleach) for 48 hours, rinsed with Milli-Q water, and treated with bleach again in an effort to remove all organic material. Samples were rinsed with 500 mL of Milli-Q water three times to remove any bleach or dissolved sulfate before dissolution of the carbonate material. Dissolution of the carbonate samples involved slowly adding 6N HCl to maintain a pH around 4 and until no reaction occurred with additional HCl. The acidic solution and insoluble residues

were rinsed with Milli-Q water and separated via centrifuge. The insoluble residues were set aside for future study of the $\delta^{34}S$ of the pyrite fraction. The remaining solution was combined with enough NaOH to raise the pH to 9-10 to cause any dissolved metals to be removed from solution (i.e., those associated with the inadvertent dissolution of pyrite). Resulting precipitates were removed via centrifuge and several drops of nitric acid (HNO_3) were added to the solution to lower the pH to ~4. Then 30 mL of 1M $Ba(NO_3)^-$ was added to form barium sulfate ($BaSO_4$) and allowed to react over the course of 48 to 72 hours. The precipitate was isolated via centrifuge, dried, weighed, and shipped to the Isotope Geochemistry Lab at the University of California - Riverside to be processed for $\delta^{34}S$ using the Delta V Plus mass spectrometer, Costech Elemental Analyzer and a CONFLO III interface.

Group 2 specimens presented an unexpected precipitation of unknown salts exhibiting blocky cleavage and forming large (> 3 cm) blocks before reducing to small (< 1 cm) crystals over a period of 24 to 48 hours. This precipitation occurred following the addition of a newly created batch of $Ba(NO_3)^-$. A small amount of the precipitate was removed from sample #258 (545.5 cumulative meters), oven dried overnight, and analyzed using a FEI Quanta FEG scanning electron microscope utilizing Bruker Quantax energy dispersive spectroscopy (EDS) software. Results across the crystal faces were variable, but exhibited consistently high concentrations of chloride. Trace amounts of sulfur, strontium, aluminum, and barium were also identified. With this knowledge, the samples were diluted further with Milli-Q water and heated to dissolve all salt constituents. An additional 30 mL of fresh $Ba(NO_3)^-$ was added, resulting in the expected precipitation of barium sulfate in the form of a white powder. Potential explanations for this anomalous behavior point to inadequate removal of the bleach solution. To test the completeness of sulfate precipitation following removal of the barium sulfate, an additional 30

mL $Ba(NO_3)^-$ was added . Small amounts of additional $BaSO_4$ powder were precipitated, indicating either a possible failure of the process due to ineffective rinsing of this particular group, or the need to adjust the amount of $Ba(NO_3)^-$ in the methodology itself. Further analysis and testing of this final step therefore is suggested.

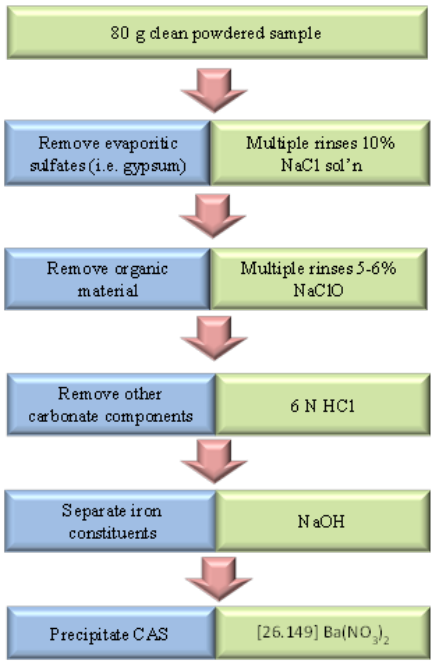

Figure 5: Flow chart displaying steps of CAS extraction (green) with their explicatory descriptions (blue). (Gill et al., 2011; Wotte, 2012; Cole Edwards, personal communication)

Scanning electron microscopy using an FEI Quanta FEG scanning electron microscope (SEM) was utilized to examine the purity of the carbonate powder prior to chemical processing. Impurities such as calcite veins and significant clay bodies were removed as best as possible with a water-based, diamond-blade saw followed by repeated sonication in a water bath to further remove impure substances. EDS investigation of powder taken from two samples (including a sample found in the present data set, located at 322 cumulative meters and one located at 479.5 cumulative meters), and mounted onto aluminum stubs and carbon-coated, revealed very pure calcium carbonate with little variation. The software employed interprets elemental compositions via x-ray spectroscopy of scattered electrons (details of beam size, etc. provided in Figure 6).

Various methods have been widely utilized and manipulated in an effort to gauge the isotopic compositions of sulfate in CAS found within ancient deposits. These methods apply a range of techniques to isolate this particular carbonate associated sulfate from alternative sulfur-deposits such as those found in gypsum and pyrite (Wotte et al., 2012). Our results add to the compilation of tests that continuously examine and refine sulfate-extracting methodologies.

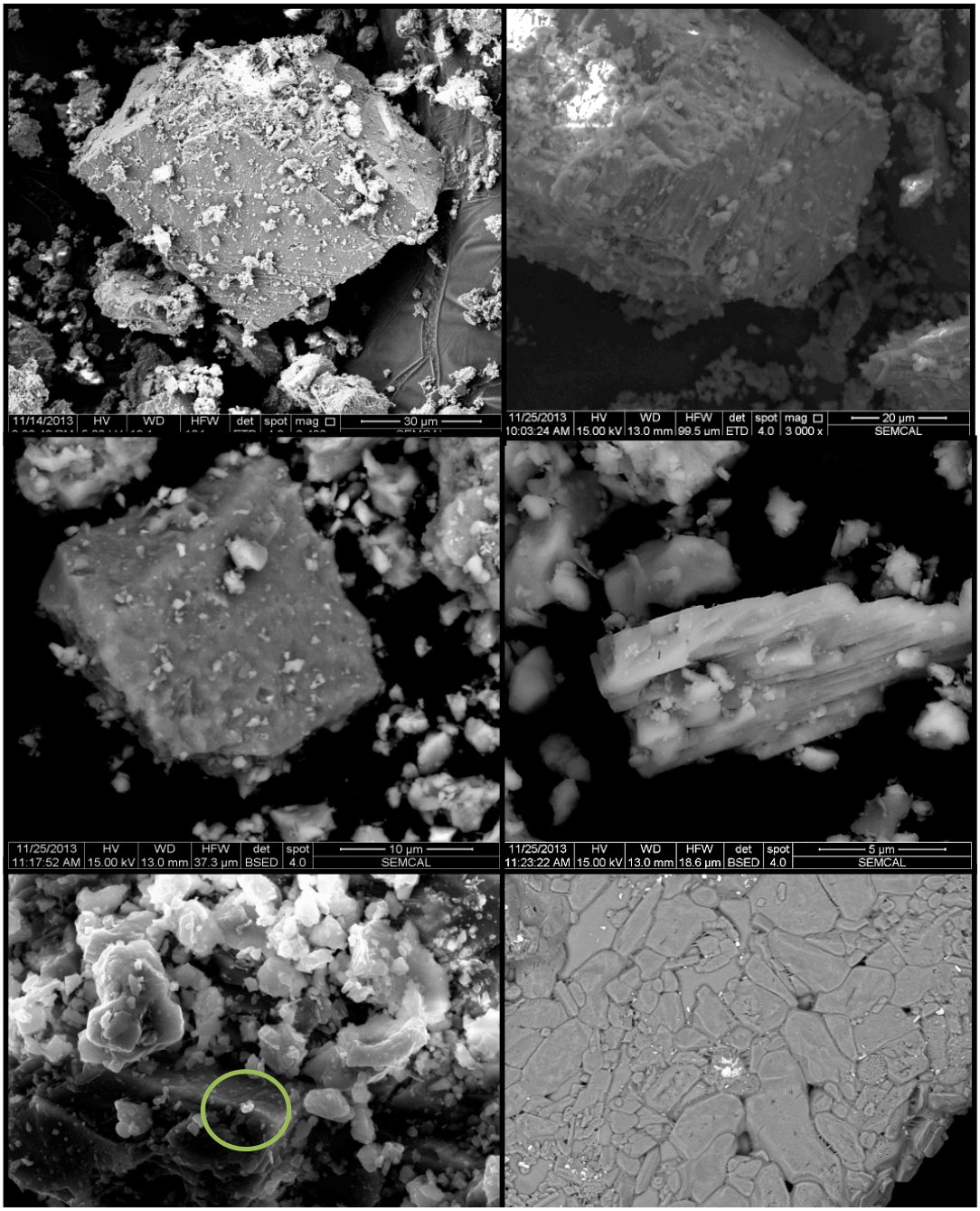

Figure 6: (top left) rhombic calcium carbonate crystal within powdered samples pre-processing. (top right) variant cleavage drawn from powdered sample pre-processing. (middle left) pure quartz crystal within pre-processed sample powder (by EDS inspection). (middle right) pure calcium carbonate (by EDS inspection). (bottom left) bright spheroid circled shows iron component. (bottom right) unknown salt precipitated after addition of barium nitrate to sample solutions of Group 2 – contains minor traces of sulfate. Further EDS analysis revealed consistently high chlorine and various low miscellaneous elemental concentrations (e.g., Na, Ba, Al, Sr), interpreted as forming a variety of salts including NaCl.

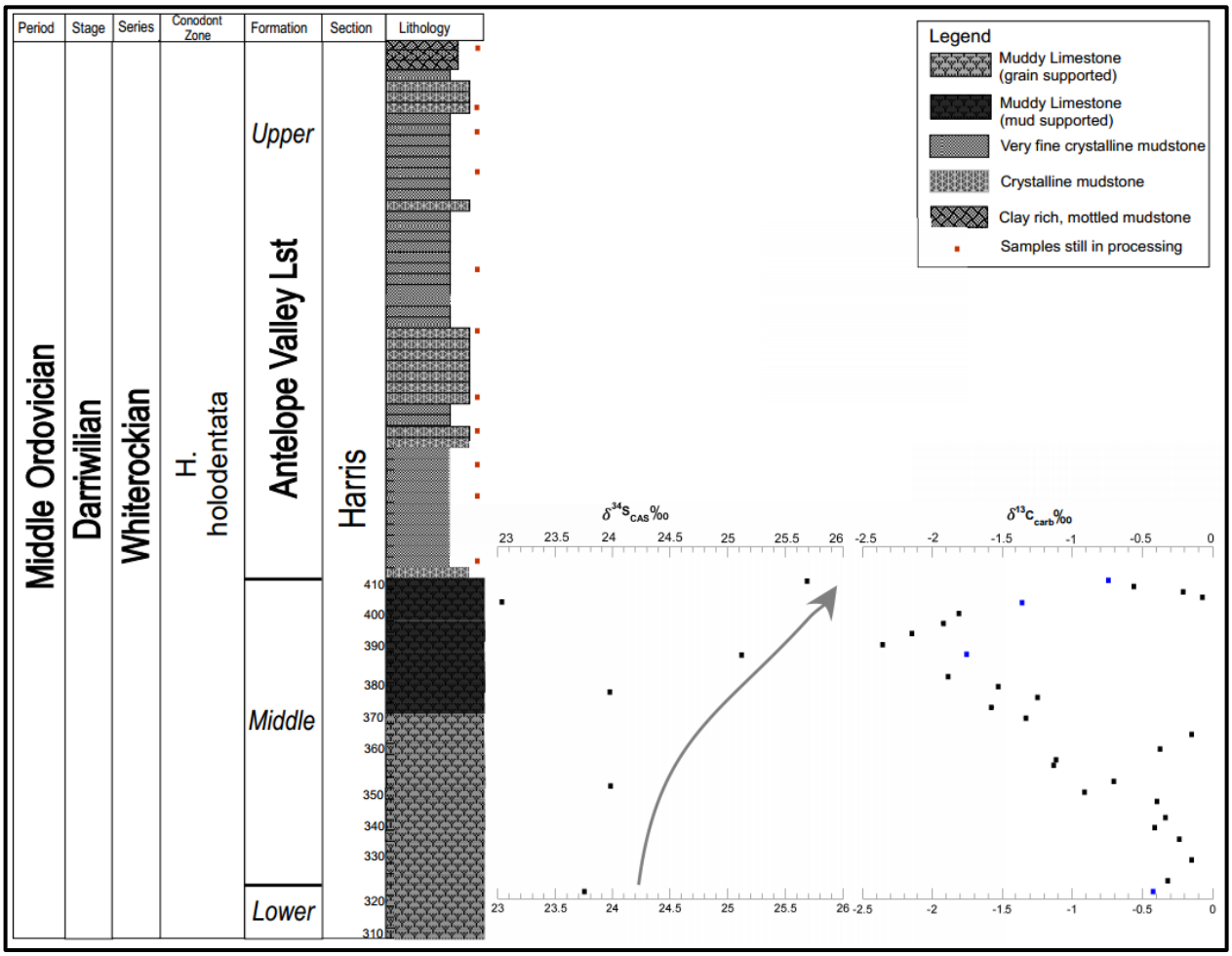

Figure 7: Stratigraphic column for the analyzed section. Each division in the visualization of the stratigraphic column lithology represents two samples in order to increase lithofacies resolution in an effort to account for the size of the data set. The large grey arrow indicates the interpreted trend of sulfate values. Blue colored data points within the $\delta^{13}C_{carb}$ data are directly correlative

Results

Results from the lower and middle members of the AVL consist of six total $\delta^{34}S_{CAS}$ data points (Figure 7). The exact trend of $\delta^{34}S_{CAS}$ appears antithetical with coeval $\delta^{13}C_{carb}$ trends. The first three $\delta^{34}S_{CAS}$ values, beginning from ~320 meters within the stratigraphic column, are roughly equivalent, with a positive excursion of 1.14‰ occurring between the third and fourth value. The succeeding values portray a sudden negative shift of - 2.09‰ over 15 meters, abruptly

followed by a positive shift of 2.66‰ over roughly 7 meters. The single $\delta^{34}S_{CAS}$ value lying outside of the positive trend observed in Figure 7 is interpreted here as an outlier. In contrast to $\delta^{34}S_{CAS}$, $\delta^{13}C_{carb}$ shows an initial negative excursion of -2.21‰ followed by an overall positive shift of 2.16‰. Excluding the outlier, $\delta^{34}S_{CAS}$ trends toward isotopically heavier values, shifting an overall total of 1.94‰, with a best fit line sloping 34.7 meters per isotopic per-mil unit change. When plotted at the same resolution, a positive correlation between $\delta^{34}S_{CAS}$ and $\delta^{13}C_{carb}$ is apparent (see Fig. 8). $\delta^{13}C_{carb}$ shows a maximum negative excursion of -2.29‰ before turning and tracking the $\delta^{34}S_{CAS}$ data in a positive excursion of sub-equal magnitude (1.61‰). The $\delta^{34}S_{CAS}$ data have a standard deviation of 0.9707, which falls within the 95% confidence interval and thus appears to be statistically robust.

Discussion

The causal mechanisms for the observed positive shift in $\delta^{34}S_{CAS}$ in the middle AVL could include: 1) an increase in bacterial sulfate reduction in the oceans (e.g. zonal euxinic/anoxic environments); 2) sea level rise and a decrease in terrestrial weathering of isotopically light sulfide; or 3) mixing of isotopically distinct water mass reservoirs of sulfur (Gill et al., 2007; Lyons et al., 2010; Edwards and Saltzman, 2014). Because the sediments here accumulated on a passive margin, tectonic controls (e.g., subsidence) on sea level are likely unimportant compared to eustatic sea level (Bond et al., 1984). An increase in seafloor spreading rates could produce a small amount of sea level rise and subsequent local drowning of the platform leading to increased pyrite burial in anoxic waters and decreased weathering inputs from the continents (Mackenzie and Pigott, 1981). However, the $\delta^{34}S_{CAS}$ trend has not been

correlated on a global scale, making the significance of mixing of heterogeneous water masses unclear.

Diamond (2013) identified a cotemporaneous increasing trend in $\delta^{13}C$, which he interpreted as representing the burial of organic material through the rise of sea level (the $\delta^{13}C_{carb}$ shift was globally correlated to the Middle Darriwilian Isotope Carbon Excursion, or MDICE). Diamond (2013) further interpreted a shift in $\Delta^{13}C$ (the isotopic difference between carbonate and organic matter) to reflect a coeval increase in atmospheric oxygen. I propose that the positive shift in $\delta^{34}S_{CAS}$ values at Meiklejohn Peak, Nevada also support this hypothesis of a rise in sea level that caused enhanced pyrite burial in the Middle Ordovician. Moreover, this suggests that the increased burial of pyrite and organic carbon led to a coincident increase in atmospheric oxygen and possibly of marine animal life.

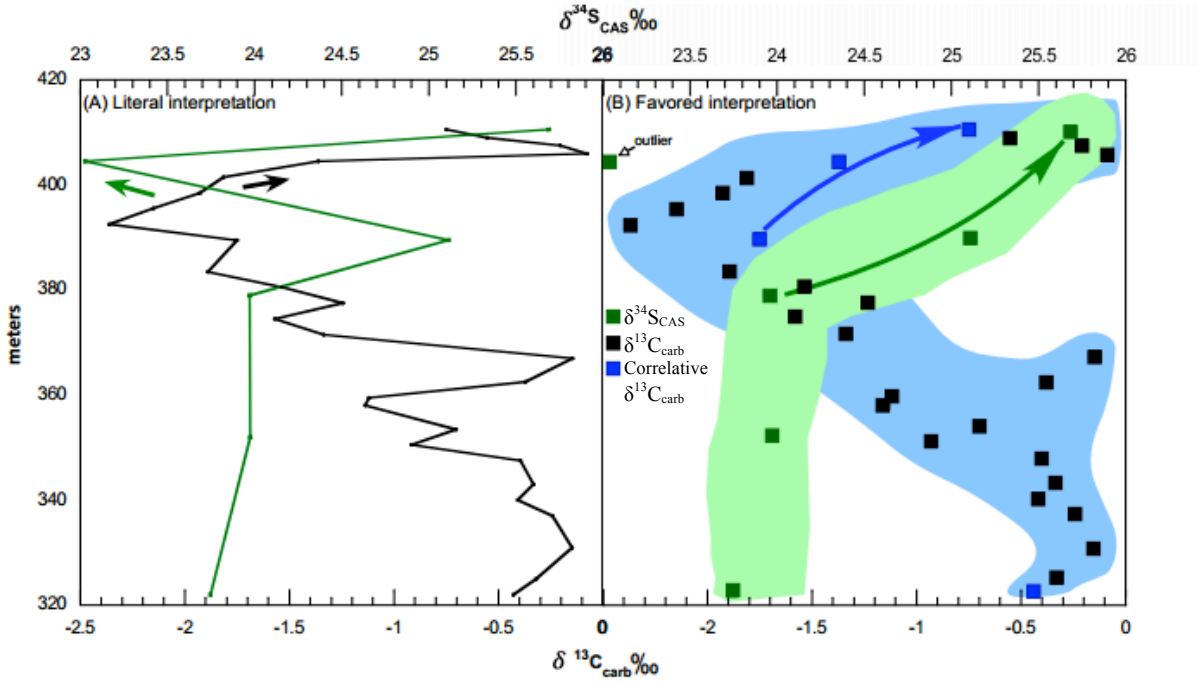

Figure 8: Two interpretations of coupling between δ34SCAS and previously collected δ13Ccarb (Diamond, 2013). (A) presents a literal interpretation of the data, incorporating every point. Arrows indicate opposing trends between δ13Ccarb and δ34SCAS. (B) presents the favored interpretation of the data, excluding the labelled outlier (upper left). General δ34SCAS trend is highlighted in green, and general δ13Ccarb trend is highlighted in blue. Blue points accentuate δ13Ccarb drawn from samples also analyzed for the corresponding δ34SCAS. Covariant carbon (blue arrow) and sulfur (green arrow) isotope trends displayed.

Conclusion

Integration of $\delta^{34}S_{CAS}$ with coeval $\delta^{13}C_{carb}$ data allows for examination of atmospheric oxygenation that may have affected biodiversification in the Ordovician. $\delta^{34}S_{CAS}$ data from Middle Ordovician strata from Meiklejohn Peak, Nevada display a positive isotopic excursion coeval with a positive excursion in $\delta^{13}C_{carb}$. This is consistent with a rise in sea level that resulted in burial of isotopically light sulfur as pyrite in sediments. Furthermore, I propose that these results support the interpretations of previous work in this section that describes a rise in sea level accompanied by an increase in burial of isotopically light organic carbon and an increase in atmospheric oxygen. The utilization of $\delta^{34}S_{CAS}$ data adds support and clarity to previous interpretations based on $\delta^{13}C_{carb}$ alone.

Suggestions for Future Research

Future analysis of these samples will add resolution to this data set, while further refining the laboratory extraction methodology utilized. Additionally, pyrite analysis upon sample residuals offers another outlook upon the biogeochemical controls on sulfur cycling throughout the study interval. An effort to compare and perhaps correlate $\delta^{34}S_{CAS}$ values globally would be beneficial to examining the extent and details of this proposed oxygenation event.

Aknowledgements

A special thanks to Dr. Matthew Saltzman for commissioning and guiding this project. Thank you to Cole Edwards for his patient laboratory supervision and to Charlie Diamond and the Isotope Geochemistry Lab under Dr. Lyons at the University of California Riverside for their aid in sample analysis. An additional thank you to Dr. Julie Sheets, Dr. David Cole, and Dr. Sue

Welch for providing use of and training in the Ohio State School of Earth Sciences Scanning Electron Microscopy Lab. This project was funded by the National Science Foundation GEOEAR #0819832.

References

Blakey, R., Middle Ordovician Mollewide paleoglobe, <http://cpgeosystems.com/470moll.jpg>, 28 February, 2014

Blakey, R., Middle Orodvician Paleographic Map of North America, <http://cpgeosystems.com/namO470.jpg>, 7 March, 2014

Bond, G.C., Nickeson, P.A., and Kominz, M.A., 1984, Breakup of supercontinent between 625 Ma and 555 Ma: new evidence and implications of continental histories: Earth and Planetary Science Letters, v.70, p.325-345.

Canfield, D.E., and Raiswell, R., 1999, The Evolution of the Sulfur Cycle: American Journal of Science, v.299, p.697-723.

Diamond, C.W., 2013, Ocean oxygenation during the Middle Ordovician: links to biodiversification?: Unpublished B.S. thesis, The Ohio State University, Columbus, Ohio.

Edwards, C.T., and Saltzman, M.R., 2014, Carbon isotope (δ13Ccarb) stratigraphy of the Lower–Middle Ordovician (Tremadocian–Darriwilian) in the Great Basin, western United States: Implications for global correlation: Paleogeography, Palaeoclimatology, Palaeoecology, v.399, p.1-20.

Gill, B.C., Lyons, T.W., and Saltzman, M.R, 2007, Parallel, high-resolution carbon and sulfur isotope records of the evolving Paleozoic marine sulfur reservoir: Paleogeography, Palaeoclimatology, Palaeoecology, v.256, p.156-173.

Gill, B.C., Lyons, T.W., and Frank, T.D., 2008, Behavior of carbonate-associated sulfate during meteoric diagenesis and implications for the sulfur isotope paleoproxy: Geochimica et Cosmochimica Acta, v.72, p.4699-471.

Gill, B.C., Lyons, T.W., Young, S.A., Kump, L.R., Knoll, A.H., and Saltzman, M.R., 2011, Geochemical evidence for widespread euxinia in the Later Cambrian ocean: Nature, v.469, p.80-83.

Harris, A. G., 1979, Conodont Color Alteration, an Organo-Mineral Metamorphic Index, and its Application to Appalachian Basin Geology: USGS, Washington, D.C. 20560, p.3-16.

Kah, L.C., Lyons, T.W., and Frank, T.D., 2004, Low marine sulphate and protracted oxygenation of the Proterozoic biosphere: Nature, v.431, p.834-838.

Lyons, T.W., and Gill, B.C., 2010, Ancient sulfur cycling and oxygenation of the early biosphere: Elements, v.6, p.93-99.

Mackenzie, F.T., and Pigott, J.D., 1981, Tectonic controls of Phanerozoic sedimentary rock cycling: The Geological Society London, v.138, p.183-196.

McFadden, K.A., Huang, J., Chu, X., Jiang, G., Kaufman, A.J., Zhou, C., Yuan, X., and Xiao S., 2008, Pulsed oxidation and biological evolution in the Ediacaran Doushantuo Formation: PNAS, v.104, no.9, p.3197-3202.

Nicholson, R.V., Gillham, R.W., and Reardon, E.J., 1988, Pyrite Oxidation in carbonate-buffered solution: 1. Experimental kinetics: Geochimica et Cosmochimica Acta, v.52, p.1077-1085.

Ross, R.J. Jr., 1977, Ordovician Paleogeography of the Western United States: USGS, Denver, Colorado 80225, p.19-38

Saltzman, M.R., 2003, Late Paleozoic ice age: Oceanic gateway or pCO2?: Geology, v.31, no.2, p.151-154.

Saltzman, M.R., Runnegar, B., and Lohmann, K.C., 1998, Carbon isotope stratigraphy of Upper Cambrian (Steptoean Stage) sequences of the eastern Great Basin: Record of a global oceanographic event: GSA bulletin, v.110, no.3, p.285-297.

Saltzman, M.R., and Young, S.A., 2005, Long-lived glaciation in the Late Ordovician? Isotopic and sequence-stratigraphic evidence from western Laurentia: Geology, v.33, no.2, p.109-112.

Webby, B.D., Paris, F., Droser, M.L., and Percival, I.G., 2004, The Great Ordovician Biodiversification Event: Columbia University Press, p.98-239.

Wotte, T., Shields-Zhou, G.A., and Strauss, H., 2012, Carbonate-associated sulfate: Experimental comparisons of common extraction methods and recommendations toward a standard analytical protocol: Chemical Geology, v.326, p.132-144.

Young, S.A., Saltzman, M.R., Foland, K.A., Linder, J.S., and Kump, L.R., 2009, A major drop in seawater $^{87}Sr/^{86}Sr$ during the Middle Ordovician (Darriwilian): Links to volcanism and climate?: Geology, v.37, no.10, p.951-954